

Comparison of various fluid-structure interaction methods for deformable bodies.

R. van Loon^{1*}, P.D. Anderson², F.N. van de Vosse³, S.J. Sherwin¹

¹ *Department of Aeronautics, Imperial College London,
South Kensington Campus, SW7 2AZ, London, UK*

² *Department of Mechanical Engineering, Eindhoven University of Technology,
P.O. Box 513, 5600 MB, Eindhoven, The Netherlands*

³ *Department of Biomedical Engineering, Eindhoven University of Technology,
P.O. Box 513, 5600 MB, Eindhoven, The Netherlands*

**E-mail: r.v.loon@imperial.ac.uk Tel: +44 (0)20 75945129*

1 Abstract

A perspective is given on fictitious domain methods for deformable bodies that exert large motions induced by unsteady flow. In these methods an Eulerian and Lagrangian formulation are employed for the fluid and solid, respectively, and both bodies are coupled using a Lagrange multiplier. This multiplier allows the solid not to be an integral part of the fluid mesh, that therefore requires no updating. Three variations of the fictitious domain method that have been published before, are compared to an ALE method in two numerical experiments and in conclusion the advantages, disadvantages and differences for the different approaches are regarded.

Keywords: fluid-structure interaction; FSI; fictitious domains; ALE; deformable solids; Lagrange multipliers

2 Introduction

In a finite element, finite difference or finite volume setting, the fluid domain is generally described in an Eulerian frame of reference obtaining solutions in grid/mesh points that are fixed in space.

Although this approach works well for a geometrically fixed fluid domain, difficulties arise when the fluid domain changes shape or when moving interfaces are present inside the domain. Typical examples are flow through flexible tubes, swimming fish, moving cilia, a functioning heart valve or a flapping flag. Different techniques have been proposed and investigated for handling moving interfaces and in particular the interfaces of an elastic solid structure embedded in a fluid.

One of the most well-known methods used to capture the interaction between structure and fluid is the Arbitrary Lagrangian Eulerian method (ALE). An Arbitrary Lagrangian Eulerian method allows arbitrary motion of grid/mesh points with respect to their frame of reference by taking the convection of these points into account as described in Hirt et al. (1974), Donea et al. (1982), Hughes et al. (1981) and many works thereafter. In the case of an FSI problem, the fluid points at the fluid-solid interface are moved in a Lagrangian way. Since the method is easy to implement, has low computational cost and is accurate, it is recommendable to use whenever possible. However, for large translations and rotations of the solid or inhomogeneous movements of the grid/mesh points fluid elements tend to become ill-shaped, which reflects on the accuracy of the solution. Remeshing, in which the whole domain or part of the domain is spatially discretised, is then a common strategy. The process of mesh generation multiple times during a computation can, however, be a very troublesome and time consuming task. Furthermore, the transfer of solutions from the degenerated mesh to the new mesh may introduce artificial diffusion, causing loss of accuracy.

Opposed to the ALE technique where the fluid-solid interface is accurately captured other types of methods do not require any changes of the fluid mesh/grid. A widely used non-boundary-fitting method for FSI applications is the immersed boundary method, which was proposed by Peskin (1972, 2002). The first models consider a finite difference grid for the fluid domain with an immersed set of non-conforming boundary points, that are mutually interconnected by an elastic law. This solid boundary interacts with the fluid by means of local body forces applied to the fluid at the position of the points. This body force imposes the kinematic constraint that the velocity in each of these solid point is coupled to the (interpolated) fluid velocity at that point. The introduction of these body forces has become the basic idea behind several non-boundary-fitting FSI methods. Throughout the years, the Immersed Boundary Method has been successfully applied in many application fields (Peskin and McQueen, 1989; Dillon and Fauci, 2000a; Zhu and Peskin, 2002; Gilmanov and Sotiropoulos, 2005).

Another method closely related to the the immersed boundary method, is the so-called ficti-

tious domain method (Glowinski et al., 1997). Unlike the immersed boundary method that was developed within a finite difference framework, the fictitious domain method evolved from the field of finite elements. Coupling is established by constraining fluid and rigid body at the interface using a (distributed) Lagrange multiplier and extending this constraint to the inner body. In the strong form the fictitious domain method is not different from the immersed boundary method, only by applying the multipliers (which represent the body forces) in the weak form the forces are imposed in a distributed manner using an integral formulation.

Based on the fictitious domain idea Baaijens (2001) proposed a fluid-solid interaction version suitable for slender bodies. In this work a fluid and solid mesh are generated independently from each other and both domains are coupled by means of a Lagrange multiplier along the boundary of the solid. The solid is described in a Lagrangian way, deforming under the acting fluid forces, while the Eulerian fluid mesh does not require updating. This method has been successfully applied in flexible heart valve simulations (De Hart et al., 2000, 2003).

A disadvantage of Baaijens' technique is that it is only applicable to slender bodies. Several extended versions have since been proposed where non-slender elastic solid bodies are coupled across the whole body instead of a boundary, which broadens the application field. The Extended Immersed Boundary Method (Wang and Liu, 2004) and the Immersed Finite Element Method (Zhang et al., 2004) describe the solid using the finite element method while the fluid is formulated using a finite difference or finite element method, respectively. The coupling is performed using the discrete dirac delta functions that find their origin in the meshless reproducing kernel particle method (RKPM). Examples include the dropping of rigid or deformable particles in a three-dimensional channel. Yu (2005) set out his version of the fictitious domain method for non-slender deformable bodies. Analysis of this approach was performed by two numerical examples: the motion of a slender solid slab in a pulsatile flow (like the one in Baaijens (2001)) and the self-sustained flapping of a slender solid in a constant flow (like in Zhu and Peskin (2002)).

The non-boundary-fitting methods have a reduced accuracy for the solution near the fluid-solid interface due to interpolation and in the ALE methods the fluid elements tend to get ill-shaped requiring difficult and expensive meshing. Therefore, another variation on the distributed Lagrange multiplier principle was proposed by Van Loon et al. (2004). A combination of the two might lessen their disadvantages without losing too much of the benefits. The approach consisted of the fictitious domain method similar to that of Baaijens, but extended with an ALE step and a local adaptive meshing algorithm for the fluid mesh (Van Loon et al., 2006). Due to the use of the

Lagrange multiplier the meshes did not have to be conforming at the solid-fluid interface, which allowed the meshing algorithm to be simple and very local. To show the improved accuracy, shear stresses along both sides of the solid were computed.

The aim of this work is to provide a comparison between different FSI methods that can be used for slender deformable bodies in a fluid. Comparing existing methods that have been presented in different works is always a tedious matter due to variations in discretisations, geometry, polynomial order or boundary conditions used in the different publications that might influence the comparison. We made an effort to restrain these parameters for a more specific focus on the FSI itself. The chosen approaches all fall within the finite element type of methods and each approach with its advantages and disadvantages will be highlighted. The more conventional ALE method and three variations of the fictitious domain methods will be considered in two numerical experiments. The fictitious domain methods are the ones earlier proposed by Baaijens (2001), Yu (2005) and Van Loon et al. (2006). This way we hope to provide more insight in the strengths and, possibly more important, the weaknesses of the various methods.

3 Methods

3.1 Governing Equations

First the governing equations for a fluid-structure interaction problem in the strong form are considered. The momentum balances that hold in fluid domain Ω^f and solid domain Ω^s are presented and, additionally, incompressibility of both media is enforced by a continuity constraint for the fluid and an volumetric constraint for the solid. The superscripts 's' and 'f' are used in this work to indicate if a quantity belongs to the solid or to the fluid, respectively.

Fluid:

$$\rho^f \frac{\partial \mathbf{u}^f}{\partial t} + \rho^f \mathbf{u}^f \cdot \nabla \mathbf{u}^f = \nabla \cdot \boldsymbol{\sigma}^f + \rho^f \mathbf{f}^f, \quad \text{in } \Omega^f \quad (1)$$

$$\nabla \cdot \mathbf{u}^f = 0, \quad \text{in } \Omega^f \quad (2)$$

$$\boldsymbol{\sigma}^f = 2\eta \mathbf{D} - p^f \mathbf{I} \quad \text{in } \Omega^f \quad (3)$$

Solid:

$$\rho^s \frac{d\mathbf{u}^s}{dt} = \nabla \cdot \boldsymbol{\sigma}^s + \rho^s \mathbf{f}^s, \quad \text{in } \Omega^s \quad (4)$$

$$\det(\mathbf{F}) = 1, \quad \text{in } \Omega^s \quad (5)$$

$$\boldsymbol{\sigma}^s = G \left(\mathbf{F} \cdot \mathbf{F}^T - \mathbf{I} \right) - p^s \mathbf{I} \quad \text{in } \Omega^s \quad (6)$$

Kinematic and dynamic constraint:

$$\mathbf{u}^s - \mathbf{u}^f = \mathbf{0} \quad \text{on } \partial\Omega^s \quad (7)$$

$$\boldsymbol{\sigma}^s \cdot \mathbf{n} - \boldsymbol{\sigma}^f \cdot \mathbf{n} = \mathbf{0} \quad \text{on } \partial\Omega^s \quad (8)$$

with \mathbf{n} the outer normal at the solid boundary.

Note that these equations can be posed regardless of the methods used to numerically model the interaction. In the above equations the symbols \mathbf{u} , $\boldsymbol{\sigma}$, \mathbf{f} , ∇ , p , \mathbf{I} , G , ρ , η and t , denote the velocity, Cauchy stress tensor, body force, gradient operator, pressure, unity tensor, solid shear modulus, density, fluid viscosity and time, respectively. The deformable solid body will be described in a Lagrangian formulation where the deformation tensor is defined as $\mathbf{F} = (\nabla_{\mathbf{n}} \mathbf{x}^s)^T$ describing the material deformation from reference configuration 'n' to the latest configuration. With the deformation rate tensor defined as $\mathbf{D}(\mathbf{u}^f) = \frac{1}{2}(\nabla \mathbf{u}^f + (\nabla \mathbf{u}^f)^T)$ the fluid behaves Newtonian. Note that unlike the solid, the fluid is described in an Eulerian manner.

A weak form is derived, but we refer to the works of Yu (2005) and Van Loon et al. (2006) for a more extensive formulation and will just present the resulting weak form including all necessary terms for the various methods.

$$\int_{\Omega^f} \rho^f \left(\frac{\partial \mathbf{u}^f}{\partial t} + (\mathbf{u}^f - \mathbf{u}_{grid}^f) \cdot \nabla \mathbf{u}^f \right) \cdot \mathbf{w}^f d\Omega^f + \int_{\Omega^f} 2\eta \mathbf{D}(\mathbf{u}^f) : \mathbf{D}(\mathbf{w}^f) d\Omega^f - \quad (9)$$

$$\int_{\Omega^f} p^f \nabla \cdot \mathbf{w}^f d\Omega^f + \int_{\Omega^s} \boldsymbol{\lambda} \cdot \mathbf{w}^f d\Omega^s = \int_{\partial\Omega^f} (\boldsymbol{\sigma}^f \cdot \mathbf{n}^f) \cdot \mathbf{w}^f d\partial\Omega^f, \quad (10)$$

$$\int_{\Omega^f} q^f \nabla \cdot \mathbf{u}^f d\Omega^f = 0,$$

$$\int_{\Omega^s} (\rho^s - \rho^f) \frac{d\mathbf{u}^s}{dt} \cdot \mathbf{w}^s d\Omega^s + \int_{\Omega^s} (\boldsymbol{\sigma}^s - \boldsymbol{\sigma}^f) : \nabla \mathbf{w}^s d\Omega^s - \int_{\Omega^s} \boldsymbol{\lambda} \cdot \mathbf{w}^s d\Omega^s = \quad (11)$$

$$\int_{\partial\Omega^s} (\boldsymbol{\sigma}^s \cdot \mathbf{n}^s) \cdot \mathbf{w}^s d\partial\Omega^s,$$

$$\int_{\Omega^s} q^s (J - 1) d\Omega^s = 0, \quad (12)$$

$$\int_{\partial\Omega^s} (\mathbf{u}^f - \mathbf{u}^s) \cdot \mathbf{w}^\lambda d\partial\Omega^s = \mathbf{0} \quad (13)$$

Symbols w and q denote the appropriate weight functions and J is the determinant of \mathbf{F} , which represents the volume change. The ∂ symbol is used to denote the boundary of a domain. Note that in Eq. (9) and Eq.(11) a Lagrange multiplier λ is introduced to enforce the kinematic constraint in Eq. (13). For the ALE approach Eq. (13) is omitted as well as the integrals associated with the Lagrange multiplier. The quantity \mathbf{u}_{grid}^f is the velocity of the grid points which is required in an ALE formulation. We point out that the term $-\boldsymbol{\sigma}^f : \nabla \mathbf{w}^s$ accounts for the stresses in the fluid underneath the solid. These stresses are assumed negligible compared to the solid stresses, a similar assumption that was made in e.g. Zhang et al. (2004) or Yu (2005). Using the same reasoning as given by Yu we neglected this integral in our formulation. The most significant difference with the works of Baaijens and Van Loon et al. is the mass term in the balance of momentum for the solid. The absence of the mass term in solid constitutive law is obtained for the parameter choice $\rho^f = \rho^s$, i.e. a neutrally-buoyant solid. Furthermore, note that the surface integral over the solid body is replaced by a line integral along the center of the solid body in these methods.

3.2 Solution methods

Although different methods are compared the computations are all done within the same framework. The finite element package SEPRAN (Segal, 2003) is used for all the computations and the matrix build-routines for the solid and fluid are identical for the different methods. Also the boundary conditions and geometry are identical, except for the constraint at the fluid-solid interface. The element type used for the fluid is $P_2^+ - P_1$ and for the solid $Q_2 - P_1$ (Bathe, 1996). The $P_2^+ - P_1$ elements are chosen because the adaptive meshing procedure is based on triangular elements. This might, however, not be the optimal element choice for the other methods. The discretisation of the fluid mesh is very similar for the different approaches To focus solely on the fluid-solid coupling, we aimed to eliminate all other factors of error between the different computations.

Note that the non-linear terms are linearised and subsequently the resulting linearised equations are solved using a Newton-Raphson scheme. A relative convergence criteria is used for the fluid as well as the solid and is defined as the iterative contribution divided by the time step contribution. The convergence tolerance is set to 10^{-6} for both the fluid and solid solution. The fluid, solid and

(if required) coupling matrices are computed and assembled in a large matrix that is solved fully coupled with a direct solver.

3.2.1 ALE

Although ALE methods are generally not restricted to a conforming fluid-solid interface, the solid and fluid mesh in our approach are generated such that mesh points are shared at the interface (Fig.1). Consequently, mesh refinement for the solid will automatically result in a refinement of the fluid mesh near the interface. The nodal points of the Eulerian mesh can be moved arbitrarily if an extra convection term for these mesh points is taken into account. Since the mesh of a Lagrangian moving solid is connected to the mesh for an Eulerian fluid, the fluid-solid interface points are moved in a Lagrangian manner at the end of each time step as illustrated in Figs. 2(a) and 2(b). This way the solid-fluid interface stays intact and solid as well as fluid solutions can be computed accurately near this interface. If only the fluid points at the interface are moved, fluid elements generally become ill-shaped with increased motion. Therefore, element-shape preserving algorithms are applied on (part of) the fluid domain. After each time step the fluid is considered to behave like a solid, i.e. an algebraic set of equations is solved each time-step, that generates the displacements and velocities of the fluid mesh points. In this work we used a compressible Neo-Hookean law defined by $\boldsymbol{\sigma}^s = \kappa(J - 1) + G/J \left(\mathbf{F} \cdot \mathbf{F}^T - J^{2/3} \mathbf{I} \right)$ to deform the fluid mesh. The outer boundaries will be fixed and a Dirichlet boundary condition is prescribed at the fluid-solid interface based on the Lagrangian motion of the solid that is computed in the FSI step of the computation. The values for shear modulus G and bulk modulus κ should be chosen smartly, i.e. a high compressible material will only deform elements near the interface and a nearly incompressible material might introduce ill-shaped elements far away from the interface. Solving a set of equations is probably not the most efficient method for mesh conservation compared to other methods like Laplacian smoothing or solving the Laplace equation (see for example Bathe and Zhang (2004)), but we found it was robust and effective. To reduce computational costs we performed only one iteration with the linearised set of equations. From the deformed fluid mesh the grid velocities can be computed.

3.2.2 Fictitious domain (FD)

Unlike the meshes used for the ALE computation, conformity between the meshes is not required in the fictitious domain methods. The solid mesh can be generated independently from the fluid

mesh and requires no alignment whatsoever as shown in Fig. 2(c). As mentioned before, the routines to build the fluid and solid matrices are identical to those used in the ALE method. The assembly of the matrices and consequently the coupling between solid and fluid, is however, different. In the fictitious domain approach the domains are coupled by introducing a Lagrange multiplier across the solid body. This multiplier imposes the kinematic constraint as given by Eq. 13 and in itself represents the body force to enforce this constraint. Since the meshes are mutually non-conforming, interpolation is required. Unlike for the ALE method, the solid and fluid matrix are non-overlapping when assembled in the larger matrix. Extra matrix blocks associated with the Lagrange multipliers provides the coupling. Baaijens (2001) introduced the idea to use the fictitious domain method, that was formerly used only with embedded rigid bodies, for slender elastic bodies in a fluid and Yu (2005) generalised the approach for non-slender bodies by introducing a formulation in which the whole solid surface was coupled (2D). One could reason that Baaijens' method is the same as that proposed by Yu with a specific choice to discretise the Lagrange multiplier. Clearly, this choice will only lead to acceptable errors for slender bodies. In this work the Lagrange multipliers will be discretised based on the solid discretisation using the middle points of the solid element edge as a collocation point to enforce the coupling (Fig.3(a)). In order to couple the entire body several coupling curves are defined across the thickness of the body, i.e. a solid body with four elements across the thickness will be coupled along five coupling curves (Fig.3(b)).

3.2.3 Combined fictitious domain and adaptive meshing (FD/adap)

The last method that will be considered basically combines the ALE and fictitious domain method with an adaptive meshing scheme. Similar to the fictitious domain method proposed by Baaijens the solid domain is embedded in the fluid domain and the coupling is enforced on one curve along the solid body. The difference lies in the adaptive meshing scheme that is applied near the solid boundary. The fluid mesh is altered such that a fluid curve consisting of elemental edges (2D) is created that coincides with the curve at which the kinematic constraint holds. Note that, although the meshes now have an overlapping curve, the fluid and solid discretisations of these curves are different. It has been shown that the introduction of this adaptive meshing scheme allows pressure jumps across this interfacial curve and increases the accuracy of the velocity field in the vicinity of the solid such that shear stresses at both sides of the interface can be computed (Van Loon et al., 2004). Like in the ALE method described above, the fluid interfacial curve is moved based

on the computed motion of the solid. Next, a new fluid mesh is generated based on the new position of the solid. Subsequently, the solutions are transferred from the old onto the new mesh, which is then used for computing the next time step. For a more elaborate description of this approach the reader is referred to Van Loon et al. (2006). Finally, we need to mention that based on the discretisation of the interfacial fluid curve discontinuous linear polynomials are used for the coupling elements (Fig. 4). Since the fluid curve changes in time the number of coupling elements is not constant, as opposed to the FD methods,

4 Results

Two numerical experiments have been performed to compare the different methods. In the first test a solid membrane embedded in a fluid is considered. With increasing fluid pressure at one side of the domain the membrane will start to bulge toward a typically circular shape. In time the solid will undergo increased stretching and consequently the ratio between the discretisation sizes between the solid fluid and/or Lagrange multipliers will change, which will influence the coupling. The second test is a self-sustained flapping of a thin solid slab that is initially aligned with the flow direction. Although constant boundary conditions are imposed to the fluid domain the solid membrane will start flapping at a constant amplitude. This makes this problem ideal for analysis, since only the FSI determines this periodic transient behaviour.

4.1 Fluid induced bulging of a membrane

In this first test a slender solid is considered that separates the fluid domain in two parts as shown in Fig. 5. The boundary conditions applied to the fluid domain read,

$$\boldsymbol{\sigma}^f \cdot \mathbf{n}^f = h(t) \quad \text{on } \Omega_1^f \quad (14)$$

$$\mathbf{u}^f \cdot \mathbf{n}^f = 0 \quad \text{on } \Omega_2^f \quad (15)$$

with $h(t)$ an increasing linear function in time. Since no flow is allowed through the membrane, an influx through Ω_1^f will cause the pressure to rise in the bottom part of the fluid domain and induce deformation of the membrane (Fig. 5). Due to the incompressibility of the fluid the amount of fluid that enters the domain will equal the amount leaving the domain, but also equal the fluid volume that is displaced by the membrane, i.e.:

$$\int_t \int_{A_{in}} \Phi_{in} dA_{in} dt = \int_t \int_{A_{mem}} \Phi_{mem} dA_{mem} dt = \int_t \int_{A_{out}} \Phi_{out} dA_{out} dt \quad (16)$$

where Φ represents the fluid flux with A the surface area. This observation can be used to analyse the functionality of the different methods and in particular for the methods with coupling imposed by Lagrange multipliers.

The coarse mesh used for the computations is shown in Fig. 6 and the corresponding dimensions of the domain can be found in table 1. The solid membrane is a flat rectangular surface consisting of 50x4 quadrilateral elements. A finer fluid mesh was also used for which the element size was reduced by a factor two. The membrane is only fixed at one point (denoted by P in Fig. 6) at each side and is therefore free to pivot. In order to spread the point forces and keep the curves at these ends straight, layers of very stiff elements are attached that do not interact with the fluid (and are not shown in the figure). The material parameters used can be found in table 2.

4.1.1 ALE

For the ALE formulation it was found that Eq. (16) holds at machine precision. Since fluid and solid nodes are shared a strong coupling is established and no errors are introduced caused by the FSI. The results for the ALE formulation can therefore be used as a reference for the FD and FD/adap method. In Fig. 5 the different stages of membrane deformation are shown and in Fig. 7 the variation of the flux in time is plotted, showing some inertial effects that damp over time. We defined a relative error as $\varepsilon_{mem}(t) = (\Phi_{mem}(t) - \Phi_{in}(t)) / \max(\Phi_{in})$ and looked how this error varied in time for different mesh configurations.

4.1.2 FD/adap

Like in the ALE computation the coupling is established along the centerline curve of the solid. The adaptive meshing scheme ensures alignment of the fluid mesh with this centerline, however, with different discretisation for the fluid and solid. The type of fluid elements used, allow for sharp pressure jumps across element edges and therefore across the membrane. Since the fluid pressure is the driving force for the membrane deformation only small differences are, therefore, obtained when comparing membrane motion with the ALE results. Even for coarse meshes the methods seems to compute sufficiently accurate results and the computations run robustly until the membrane crosses the upper boundary. However, in time, error ε_{mem} varies randomly (Fig. 8) and is of the order 10^{-5} for the mesh presented in Fig 6. For a fluid mesh twice as fine this error reduces the average error by a factor of five. The error variations are most probably related to the mapping procedure. Nonetheless, the method seems to produce good results for this type

of problem in solid motion as well as fluid flow.

4.1.3 FD

As mentioned before, no fluid mesh changes are required in contrast to the former methods. The coupling was established in five layers or in one layer along the centerline of the solid as was explained in Fig. 3. All FD computations stopped before reaching the deformation levels of the ALE and FD/adap due to a non-converging solution. Since the Lagrange multiplier represents the traction force between solid and fluid, the choice for the coupling points, results in point forces. This causes some oscillations in the solid that might impede convergence.

The general trend for the error ε_{mem} was that initially values of the same order as for the FD/adap method were found, but in time increased with artificial leakage as result. Interestingly enough, the errors are not caused by the solid displacements but by seemingly arbitrary fluctuations in time of the fluid inflow. The solid motion was smooth and difference in Φ compared to the ALE solution were small (Fig. 7). Tests where the deformed membrane and the fluid pressure reached a steady-state equilibrium showed no leakage.

The FD method is known not to capture the velocity and pressure field near the coupled boundary accurately and for coarse fluid meshes it might in time influence the whole fluid velocity field. For the fluid mesh of Fig. 6 the worst results were found. The fluid field was far from symmetric and the membrane motion did not resemble that in the ALE computation. Refinement of the solid mesh to 150x4 and as a result an increase of the number of coupling elements improved the results considerably such that the motion of the membrane was captured according the ALE solution. However, the accuracy of the flow field was still poor. Refining the fluid mesh by a factor of two showed some improvement, but the flow field became only symmetric after another refinement of a factor two.

The ratios between fluid element size, solid element size and coupling element size plays an important role in the FD methods. The errors are larger for solid discretisations of 50x4 than 150x4 and with five coupling layers give smaller errors than with only one layer. The size of the fluid elements compared to the solid elements is therefore equally important as the number of coupling elements/points per fluid element.

4.2 Self-sustained flapping of a solid slab

The second test case that is considered involves higher flow rates and a less restrained solid body. The self-sustained flapping of a solid slab has been studied before using numerical codes (Zhu and Peskin, 2002; Yu, 2005) and is a good test for testing the FSI approaches. A rectangular fluid domain is considered with a thin solid slab positioned in the middle of the domain that is aligned in the flow direction (Fig. 9). The corresponding dimensions of the fluid domain and the solid body are presented in table 1. At the left boundary of the domain a constant velocity with uniform profile will be prescribed and at the right boundary the fluid flows out freely. A no-slip condition is applied along the upper and lower boundary. The solid slab was fixed in space at its left boundary and to initiate the oscillations a disturbance of the alignment of the solid was introduced by applying an upward boundary force at the first 10 time steps. As shown in Yu (2005) the amount of disturbance does not influence the final stable state, in which the solid will oscillate with constant amplitude. The relevant quantities used for the computations are shown in table 2. The simulation time T was sufficient for the solution to become stable. Note that the solid was not neutrally-buoyant for this test since inertial effects for the solid are essential for the self-sustained oscillations to occur (Zhu and Peskin, 2002).

4.2.1 ALE

The material parameters and boundary conditions for this numerical experiment were chosen such that the displacements of the solid body did not cause the ALE to fail due to collapsed fluid elements. The mesh shown in Fig. 9 was the coarsest mesh used for the ALE computations. To prevent ill-shaped elements downstream of the solid the horizontal thin band of fluid elements attached to the solid tip is prescribed to follow the computed tip displacement in y -direction at each time step. Since motion of the solid is mainly up and downward we chose to check convergence by reducing the mesh size only in y -direction and keep the number of solid elements constant. In table 3 the amplitude is shown for different mesh sizes, where Mesh1 is shown in Fig. 9. For Mesh2 and Mesh3 the number of fluid elements in y -direction is subsequently doubled. However, for the ALE computations the refinements did not seem to have a large impact on the amplitude found. A fine fluid discretisation along the solid boundary to capture the pressure gradients in that direction seems sufficient to get a spatially converging solution.

4.2.2 FD/adap

The FD/adap method shows a different behaviour than the ALE approach (Table 3, since lower values for the amplitude are obtained for the coarser meshes. An explanation for this might be that the amount of elements above and below the solid changes in time. When the solid is in an upward position there are only few elements left between the solid and the wall to capture the pressure gradients that are pushing the leaflet back down. The pressure gradients will be smoothed over the elements, which will reduce the downward force. Another reason might be that with the reorientation of the slab toward the vertical direction the discretisation of the adapted interfacial fluid curve as described in Section 3.2.3 becomes coarser toward the solid tip. Since the coupling elements are discretised based on this curve, this could result in less accurate coupling near the solid tip.

4.2.3 FD

Again two coupling approaches for the FD methods are considered. One with coupling points along the centerline and one with three layers of coupling points across the body. The results for the computation that used Mesh1, shows the most apparent difference between both approaches. While the coupling across the entire body leads to an amplitude of 0.5, coupling along the centerline results in an amplitude of 0.0. The initial offset does not provide sufficient energy to initiate the self-sustained oscillations in the case of weaker coupling. Furthermore, we found that no constant periodic solution was obtained if the fluid mesh was too coarse (Table 3). From one oscillation to another the amplitude varied by values up to 0.02. However, an increased mesh resolution solved this problem.

No general trend was found for the convergence and if 0.43 is a converged solution it is not clear why it is different from the value 0.35 found for the ALE and FD/adap methods. We do, however, realise that the number of computations performed, was limited. The sensitivity of the FD method to changes in discretisation and polynomial order of the coupling elements is, therefore, a topic of interest in the future and should be understood better to make the method more reliable.

5 Discussion

With this work we made an effort to present three different Fictitious Domain approaches that have been published before and to provide a comparison with an ALE method by means of two

numerical experiments. It was attempted to lay out the main concerns for the various approaches in setting up a numerical experiment and additionally to give an impression of their performance. A short discussion will be given about some important aspects concerning the FSI models.

5.1 Fluid-solid coupling

The ALE method clearly provides the strongest coupling since fluid and solid share nodes at the solid boundary. Therefore, it can be expected that this method will outperform the FD methods within the limits of its applicability. A slightly weaker coupling is found for the FD method with adaptive meshing (FD/adap). However, due to alignment of the fluid and solid mesh at their interface only interpolation of velocities is required along this interface. In the FD methods any alignment between the fluid and solid mesh vanishes and the weakest coupling is obtained. The distribution and amount of points across the solid at which the fluid and solid are coupled has a large influence on the results. It should be noted that we restricted ourselves to coupling using a point collocation method. Other choices are possible, like for example the bi-linear coupling elements used by Yu (2005), that might provide a more robust and accurate coupling.

5.2 Accuracy

Closely related to the fluid-solid coupling is the accuracy of the solution. In general one could say, the stronger the coupling the more accurate the solutions will be. Both test cases the solutions show the most accurate results for the ALE approach and the least accurate results for the FD approach, at a given mesh size. Due to the mesh-alignment at the solid boundary for the ALE and FD/adap method, a sharp interface defined that divides the fluid domain. In the case of slender bodies pressure jumps can be captured and the velocity field at one side of the interface does not interfere with the velocity field at the opposite side. In contrast the fluid elements are crossed randomly by the solid boundary in the FD methods and although kinematic and dynamic constraints might hold, that are imposed at the solid boundary, the necessary interpolation will reduce the accuracy in the vicinity of the boundary. However, depending on the fluid mesh size this can be a very local phenomenon and the overall flow field can be computed sufficiently accurate. Furthermore, a reduced accuracy for the fluid velocity does not necessarily influence a correct computation of the solid motion as demonstrated in Section 4.1.

5.3 Meshing

The main advantage of the FD method is that mesh generation is only required prior to the computation and that the fluid and solid mesh can be generated separately. Therefore a regular mesh can be adopted for the fluid mesh. Furthermore, no mesh changes occur during the computation except for the Lagrangian updating of the solid. With the FD/adap approach a remeshing algorithm is introduced, that adapts the fluid mesh near the boundary of the solid. Since the solid and fluid mesh do not have to be mutually conforming the algorithm is computationally inexpensive. However, the meshing algorithm we used is restricted to triangular elements that are less accurate than their quadrilateral counterparts. And although the method is robust when applied along smooth boundaries, non-smooth solid boundaries cannot be captured accurately with the current algorithm. The ALE approach as applied in this study required mutually conforming meshes for the solid and fluid. Furthermore, the Lagrangian motion of the Eulerian fluid mesh must be computed. The test cases were chosen such that a mesh preserving algorithm was a necessity, which can become computationally costly depending on the discretisation of the fluid mesh. Note that the motions of the solid were large but kept within the limits to prevent remeshing.

5.4 Implementation issues

For all methods the fluid and solid matrices are built identically. Beside that, each method has its own typical requirements. The ALE method has an intrinsic coupling and only requires a routine to update the fluid mesh after each time step. The FD method requires an extra matrix-build routine to compute the coupling matrices corresponding to the degrees of freedom that are related to the Lagrange multiplier. Furthermore, a search routine is required that determines what fluid element should be used for the interpolation in a coupling point. Finally, the FD/adap method is probably the most labour intensive since it involves the adaptive meshing algorithm, a matrix-build routine for the coupling matrices, an element searching routine, an ALE mesh-update routine and a mapping routine. From this point of view this approach is probably the least favourable.

5.5 General conclusion

Depending on the problem a suitable FSI method should be chosen. The ALE method should probably be preferred over the other approaches as long as no remeshing is required. The algorithm is robust, accurate and no extra degrees of freedom are introduced. However, as deformations,

displacements or rotations of the solid body become larger the FD methods become a sensible choice. Depending how accurately solutions need to be one could choose to use the FD/adap approach. Note that the test cases in this study only considered slender bodies, but all approaches could be used for non-slender 2D or 3D bodies.

5.6 Acknowledgement

The first author is funded by "Human Resources and Mobility" within the sixth framework program by means of a Marie Curie Intra-European Fellowship.

References

- F.P.T Baaijens. A fictitious domain/mortar element method for fluid-structure interaction. *Int. J. Num. Meth. Fluids*, 35(7):743–761, 2001.
- K.J. Bathe. *Finite element procedures*. Prentice Hall, 1996.
- K.J. Bathe and H. Zhang. Finite element developments for general fluid flows with structural interactions. *Int. J. Num. Meth. Engng.*, 60:213–232, 2004.
- J. De Hart, G.W.M. Peters, P.J.G. Schreurs, and F.P.T Baaijens. A two-dimensional fluid-structure interaction model of the aortic valve. *J. Biomech.*, 33(9):1079–1088, 2000.
- J. De Hart, G.W.M. Peters, P.J.G. Schreurs, and F.P.T Baaijens. A three-dimensional computational analysis of fluid-structure interaction in the aortic valve. *J. Biomech.*, 36(1):103–112, 2003.
- R. Dillon and L.J. Fauci. An integrative model of internal axoneme mechanics and external fluid dynamics in ciliary beating. *J. Theor. Biol.*, 207:415–430, 2000a.
- J. Donea, S. Giuliani, and J.P. Halleux. An arbitrary lagrangian-eulerian finite element method for transient dynamic fluid-structure interactions. *Comp. Meth. Appl. Mech. Eng.*, 33:689–723, 1982.
- A. Gilmanov and F. Sotiropoulos. A hybrid cartesian/immersed boundary method for simulating flows with 3d, geometrically complex, moving bodies. *J. Comp. Phys.*, 207:457–492, 2005.

- R. Glowinski, T.-W. Pan, and J. Périaux. A lagrange multiplier/fictitious domain method for the numerical simulation of incompressible viscous flow around moving rigid bodies: (i) case where the rigid body motions are known a priori. *C. R. Acad. Sci. Paris*, 25(5):361–369, 1997.
- C.W. Hirt, A.A. Amsden, and J.L. Cook. An arbitrary lagrangian-eulerian computing method for all speeds. *J. Comp. Phys.*, 14:227–253, 1974.
- T.J.R. Hughes, W.K. Liu, and T. Zimmerman. Lagrangian-eulerian finite element formulation for incompressible viscous flow. *Comp. Meth. Appl. Mech. Eng.*, 29:329–349, 1981.
- C.S. Peskin. The immersed boundary method. *Acta Numerica*, 11:479–517, 2002.
- C.S. Peskin. Flow patterns around heart valves: a numerical method. *J. Comp. Phys.*, 10:252–271, 1972.
- C.S. Peskin and D.M. McQueen. A three-dimensional computational method for blood flow in the heart i. immersed elastic fibers in a viscous incompressible fluid. *J. Comp. Phys.*, 81:372–405, 1989.
- A. Segal. *SEPRAN Introduction, User’s Manual, Programmer’s Guide, Standard Problems*. Ingenieursbureau SEPRAN, Leidschendam, 2003.
- R. Van Loon, P.D. Anderson, J. De Hart, and F.P.T. Baaijens. A combined fictitious domain/adaptive meshing method for fluid-structure interaction in heart valves. *Int. J. Num. Meth. Fluids*, 46:533–544, 2004.
- R. Van Loon, P.D. Anderson, and F.N. Van de Vosse. A fluid-structure interaction method with solid-rigid contact for heart valve dynamics. *J. Comp. Phys.*, *Accept.*, 2006.
- X. Wang and W.K. Liu. Extended immersed boundary method using fem and rkpm. *Comput. Meth. Appl. Mech. Engrg.*, 193:1305–1321, 2004.
- Z. Yu. A DLM/FD method for fluid/flexible-body interactions. *J. Comp. Phys.*, 207:1–27, 2005.
- L. Zhang, A. Gerstenberger, X. Wang, and W.K. Liu. Immersed finite element method. *Comput. Meth. Appl. Mech. Engrg.*, 193:2015–2067, 2004.
- L. Zhu and C.S. Peskin. Simulation of a flapping flexible filament in a flowing soap film by the immersed boundary method. *J. Comp. Phys.*, 179:452–468, 2002.

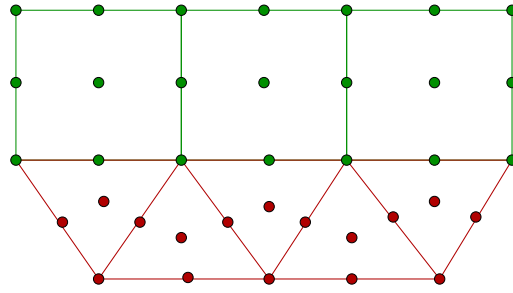


Figure 1: *The mesh computed for the ALE computations consists of shared fluid-solid nodes. This ensures a strong coupling in the FSI.*

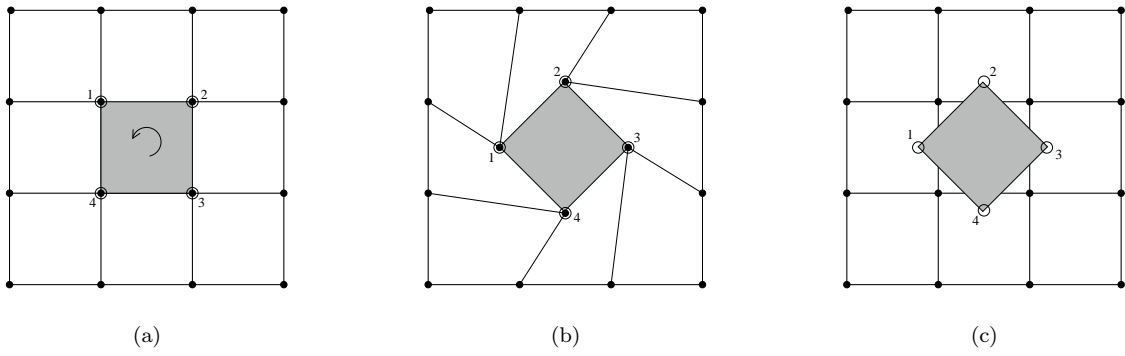


Figure 2: *Schematic representation of an ALE (b), and fictitious domain (c) method. Starting from (a) rotation of the solid gray body leads to (b) or (c) depending on the method used.*

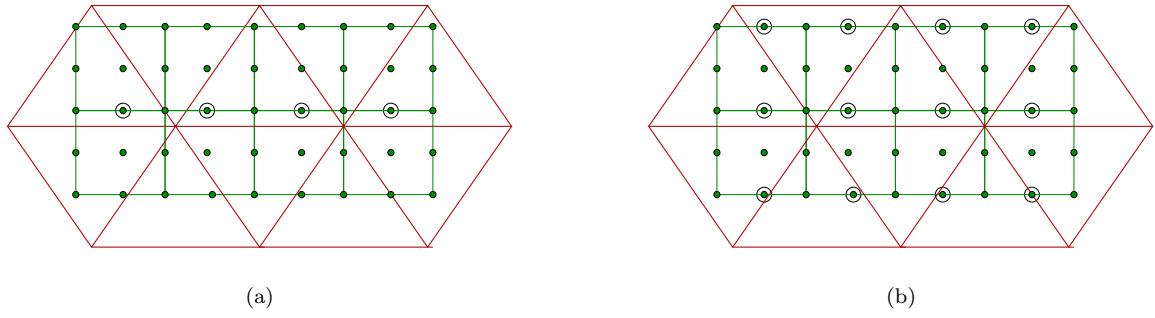


Figure 3: *The quadrilateral solid mesh is coupled to the triangular fluid mesh in collocation points (denoted by \circ) using the solid discretisation. Plot (a) shows the discretisation along the centerline curve of the solid and plot (b) shows the collocation points for coupling across the entire body.*

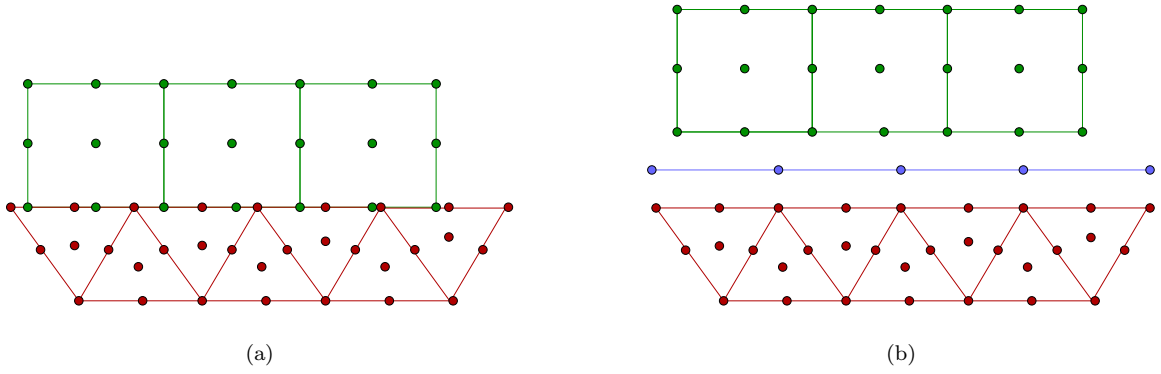


Figure 4: *Plot (a) shows the non-conforming meshes for the fluid and structure in the FD/adap approach. Along the interface the coupling elements will have the same discretisation as the fluid as shown in plot (b).*

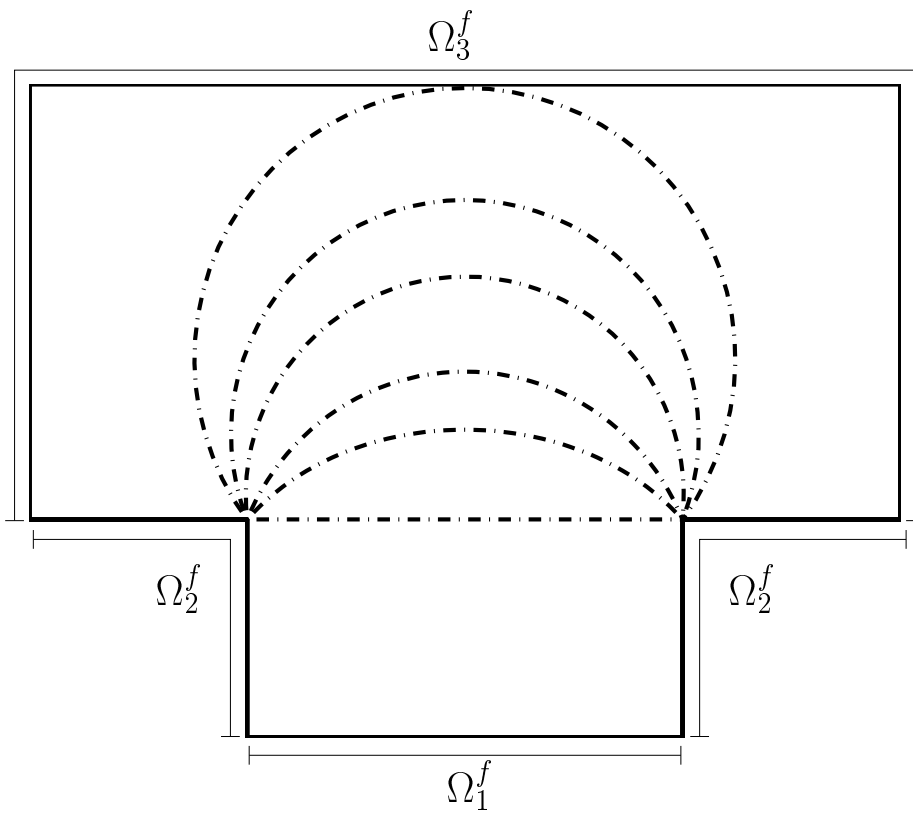


Figure 5: *Fluid induced deformations of a membrane (dashed lines) at several time points.*

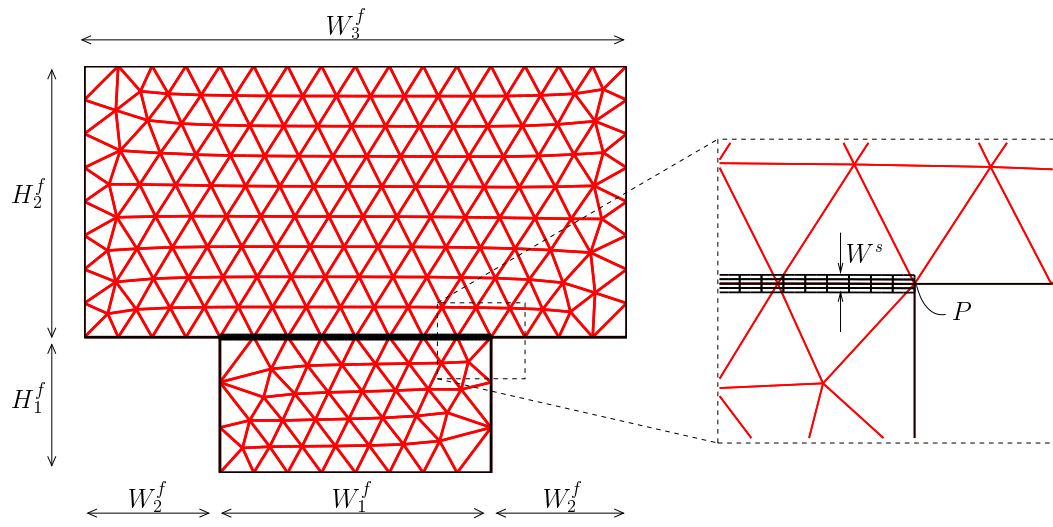


Figure 6: *The mesh and the corresponding dimensions for a membrane embedded in a fluid.*

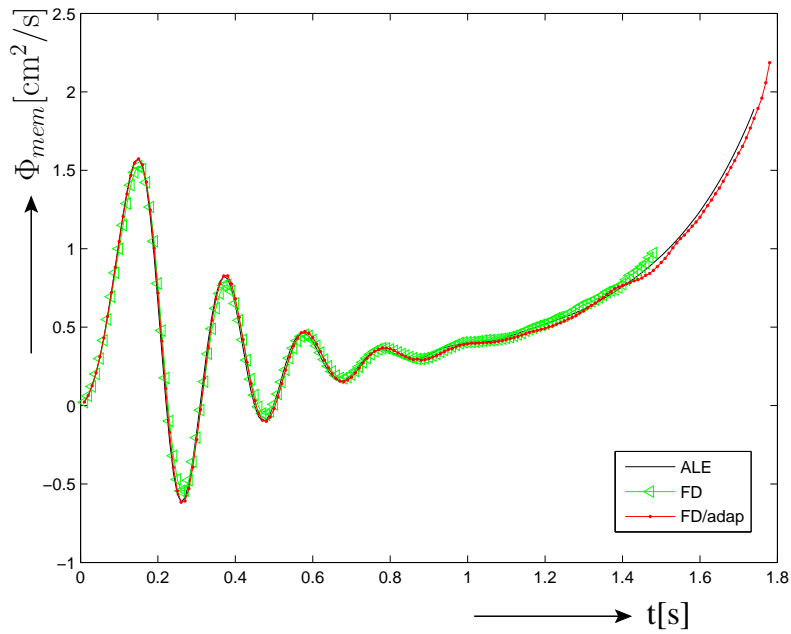


Figure 7: Fluid flux Φ_{mem} measured at the membrane interface as a function of time. A comparison between the ALE, FD and FD/adap method using the fluid mesh of Fig. 6. Note that a solid mesh of 150×4 was required for the FD method compared to 50×4 for both other approaches.

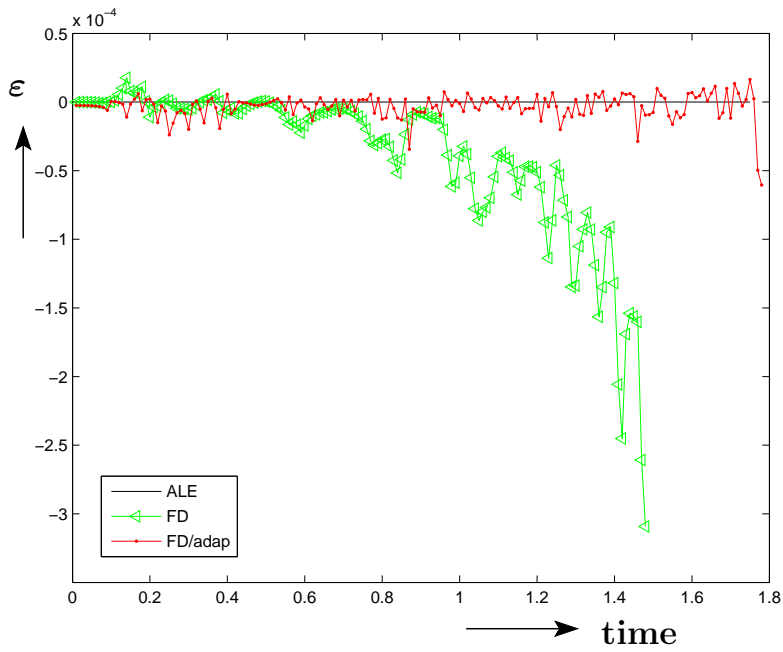


Figure 8: *The relative error ε in fluid flux at the membrane interface compared to the inlet flux with $\varepsilon = (\Phi_{mem}(t) - \Phi_{in}(t)) / \max(\Phi_{in})$.*

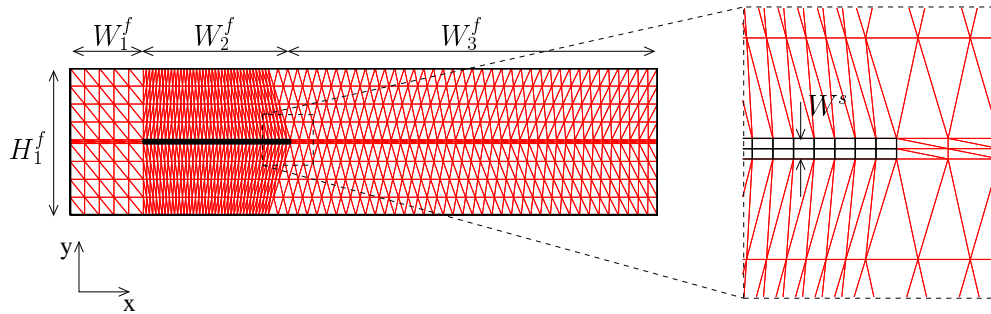


Figure 9: *The mesh and the corresponding dimensions for a solid slab embedded in a fluid.*

Table 1: Relevant geometric parameter values

	W_1^f (cm)	W_2^f (cm)	W_3^f (cm)	H_1^f (cm)	H_2^f (cm)	W_s (cm)
Num. Exp. 4.1	1.0	0.5	2.0	0.5	1.0	0.016
Num. Exp. 4.2	1.0	2.0	5.0	2.0	–	0.05

Table 2: Relevant parameter values for the numerical experiments.

	u_{max} (m/s)	p_{max} (Pa)	η (Pa s)	ρ^f (kg/m ³)	ρ^s (kg/m ³)	T (s)	G (MPa)
Num. Exp. 4.1	–	8.0	4.0×10^{-3}	10^3	10^3	2.0	100
Num. Exp. 4.2	20.0	–	4.0×10^{-3}	10^3	$11 \cdot 10^3$	2.0	50

Table 3: Amplitudes of oscillations for different mesh sizes. (* non-constant amplitude)

	Mesh1	Mesh2	Mesh3	Mesh4
ALE	0.36	0.35	0.35	-
FD/adap	0.27	0.33	0.35	-
FD (body)	0.5*	0.42	0.43	0.35
FD (line)	damps	0.43*	0.30	-

Reviewer 1

1. We disagree that the Crouzeix-Raviart elements used in this paper do not satisfy the local conservation of flux. Since the weight functions related to the continuity equation and corresponding pressure variables are discontinuous for these types of elements, mass conservation is enforced over the element (see: Fortin, *Int. J. Num. Meth. Fluids*, 1981). We do acknowledge that the elements described in Bathe's 2002 paper enforce a local conservation of momentum, where the Crouzeix-Raviart elements do not, but we do not think that this introduces substantial errors in the test cases considered.
2. Using a solid material law is indeed not the most efficient way to update the fluid mesh. Although we did not encounter any stability issues for the test problems presented, we recognise that solving a Laplace problem is more efficient, robust and therefore widely used. It is also no necessity to use a conforming fluid-solid interface as clearly illustrated in the reference papers mentioned. However, our main interest was the functionality/accuracy of the fictitious domain approaches. The ALE problem was set up to provide a reference state. We incorporated the references mentioned by the reviewer and added the here described comments on in Section 3.2.1.
3. The reference to the book has been incorporated in Section 3.2 on page 6.
4. ALE methods have been extensively and successfully used for fluid-structure interaction problems in 2D as well as 3D. The method proposed by Baaijens (see reference list) has been implemented in 3D and used for aortic heart valve models by De Hart (see reference list). The 3D code is validated using reduced 2D experimental models considering a rigid valve [Stijnen et al., *J. Fluid and Struct.*, 2004]. Finally, the fictitious domain approach combined with adaptive meshing has also been published in 3D [Van Loon et al., *C.R. Mecanique*, 2005] including a comparison of full 3D and axisymmetric 3D finite element models. In conclusion, we can say that each of the methods has been extended to three dimensions, although their performance has not been tested extensively.
5. Several typos have been removed and we rephrased some sentences.

Reviewer 2

The variational formulation Eqs (10)-(12) does indeed not incorporate the terms related to the stresses of the fluid in the solid domain. In the first paragraph of page 4 we shortly mention that this term was neglected in our models. Reason for this is that the elastic forces will dominate the fluid forces in this domain. A same reasoning can be found in and Zhang/2004 and Yu/2005 (see reference list).

For sake of clarity we have altered the formulation incorporating the stress term, which is then complete. Thereafter an explanation is given for neglecting the term in the implementation in the first paragraph on page 6. In addition we incorporated some of the references mentioned by the reviewer in our introduction.

Reviewer 3

1. Changed accordingly.
2. Indeed stress equilibrium at the fluid-solid interface should be added as an extra constraint. For the ALE formulation used in this work this requirement is fulfilled automatically by taking conforming meshes and solving the coupled system implicitly. For the fictitious domain methods the introduced Lagrange multiplier represents the traction forces between the fluid and the solid, which ensures the stresses to be in balance. We added the constraint to the governing equations on page 5.
3. We included a reference to SEPRAN.
4. We agree that an ALE method does not restrict one to conforming meshes. In the ALE approach presented, however, we did restrict ourselves to conforming meshes. We made adjustments in section 3.2.2 to clarify that ALE is not restricted to conforming meshes.
5. We removed the second "will".
6. We removed the brackets.
7. We defined the boundary conditions in a less ambiguous manner.
8. We changed the indexes.
9. We took the maximum Φ_{in} as a fixed reference to compute the relative error.

10. The solution vector can be split into a fluid and solid part with corresponding convergence criteria. In the non-converging cases it was the solid convergence criteria that was not met. For clarity's sake we omitted the word "solid".
11. The suggested plot has been incorporated and the corresponding references to the plot are substituted in the text.
12. 'have' was changed to 'has'.
13. Clearly, accuracy and meshing are closely related and an adaptive refinement would indeed also be efficient in the fictitious domain approach. However, in an effort to present the differences between the methodologies we made a subdivision in Section 5.1-5.4 and considered solely mesh generation and adaptation in 5.3 separate from the accuracy issue (Section 5.2).
14. The ΔV at the fluid-solid interface was plotted. However, error (ε) is very small as shown in the newly added figure and, therefore, plotting ΔV at the inlet or outlet would give an identical plot. Note that in processing the revisions, we replaced ΔV by the flux $\Phi = \Delta V / \Delta t$ (where Δt is the time step)
15. In table 2 we changed parameter H_1^f by H_2^f .
16. The word 'meshes' is omitted.